Correlation between Thermal Treatment and Phase Transformation in Nanocrystalline Stabilized Zirconia

Tajudeen Oladele AHMED[1*], Patrick Ovie AKUSU[1], Sunday Adesunloye JONAH[2], and Nasiru RABIU[1]

[1]*Department of Physics ABU, Zaria, Nigeria.* [2]*Centre for Energy Research and Training, ABU, Zaria, Nigeria.*
E-mail(*): tajahmol@yahoo.co.uk, tajahmol@abu.edu.ng
[*]Corresponding author: Phone: +2348065650851; Fax:08123459676

Abstract

Stabilized zirconia produced via wet chemistry has chemically higher uniformity and purity. However, the grain size, particle shape, agglomerate size and specific surface area can be modified within certain degree by controlling the precipitation and sintering conditions. Generally, any physical or chemical difference between phases or effect occurring on the appearance or disappearance of a phase can be determined via thermal analysis and X-ray Diffractometry coupled with electron microscopy. In the last few decades, these materials have received tremendous attention globally in the field of defect solid-state devices. However, the challenge in this field of research has been to study thermal behaviour of these electrolytes during phase transformations and develop improved electrolytes with low activation temperature in the range of 600°C-800°C. In this paper, we report the wet chemistry of bismuth oxide stabilized zirconia having high experimental yield and low transformation temperature. Thus, the phase transformation from amorphous Zirconia to monoclinic is reported to begin above 600^{o}C to an optimum temperature of 700^{o}C. After calcination at 800^{o}C for 4h, the powder have narrow particle size distribution in the range of 63-101µm. The average crystallite sizes of the synthesized powders range from 8-33nm.

Keywords

Stabilized zirconia; TGA-DSC; sintering-temperature; Phase transformation; XRD; SEM-EDS.

Introduction

Pure zirconia has a high melting point (2700°C) and a low ionic conductivity. However, when produced via wet chemistry by addition of monovalent-trivalent metal oxides such as CaO, MgO, Y_2O_3, La_2O_3, and Bi_2O_3 etc., the crystallization temperature is decreased and the powder produced have nanosize particles with improved ionic conductivity. As such, stabilized zirconias produced via such route are increasingly playing essential roles in defect solid-state devices from their use as electrolytes in solid oxide fuel cells (SOFCs), in oxygen sensors, super capacitors, as gas separation membranes, as gate dielectrics to hybrid solid electrolytes system for power generation [1]. However, a major problem thwarting the emergence of these devices is the high operating temperature associated with the commonly used yttria stabilized zirconia. The challenge in this field of research has been to develop alternative electrolytes to replace yttria-stabilized zirconia, in order to reduce the operating temperature from 1,000°C down to the range of 600°C-800°C. In an attempt to lower the operating temperature of YSZ, alternative electrolytes (e.g doped-CeO_2 and certain perovskites such as the only recently discovered $LaGaO_3$) with high oxygen ion conductivity have been investigated [2-6]. However, these novel materials have been found to be unstable under the prevailing reducing atmosphere at the anode side of SOFC.

Recent studies on dysprosia and scandia stabilized zirconias in this temperature region by [7-9] have been successful, with achievement of much higher ionic conductivity when zirconia was doped with Scandia. Studies on phase transformations employing DTA/DSC and TGA on zirconia based materials have shown that the phase transformation from amorphous zirconia to higher symmetry forms occurred at intermediate temperature range of 450°C – 800°C [9-12]. The activation temperature for such materials lies in this intermediate temperature range as reported by [9]. In line with such interest on zirconia-based materials, we report investigations on synthesis, phase transformation, microstructures and crystallographic structures of the synthesized nanocrystalline bismuth oxide stabilized zirconia electrolytes.

Materials and Method

Starting materials used for this synthesis are zirconium chloride octa-hydrate ($ZrOCl_2.8H_2O$, 99.5% purity, BDH Poole, England),bismuth oxychloride (BiOCl, 99.5% purity, BDH Poole, England) and sodium hydroxide (NaOH, 96% purity, May & Baker, Nigeria). Zirconylchloride and Bismuthoxychloride were dissolved in distilled water at room temperature and boiling dilute HCl respectively, until a clear solution is obtained. The co precipitation of Bi_2O_3 and ZrO_2 was obtained by mixing an appropriate concentration of dopant (Bi_2O_3) and matrix ZrO_2 in a beaker, followed by partial neutralization with NaOH solutions and precipitation of the desired oxides species. The co-precipitation reaction is as follows:

$$ZrOCl_2.8H_2O_{(aq)} + 2BiOCl_{(aq)} \xrightarrow{NaOH} (ZrO_2.Bi_2O_3)_{(s)} + 6H_2O_{(l)} + 4HCl_{(g)}$$

The sodium hydroxide/Zr^{4+} (Bi^{3+}) mole ratio (R) has significant influence on the precursor properties and the only achievable range for spherical nano-particles is $2.0 < R \leq 3.0$.

The resulting solid solution was filtered using Whattman- 12.5cm filter paper and washed several times with distilled water and solutions of ammonia and propanol until the pH of the washing solution is 8.0. The co-precipitated powder was dried at 200°C in air for 4h. Thermal analyses (Differential Scanning Calorimetry-DSC and Thermo gravimetric Analysis-TGA) were carried out on the dried powders to determine optimal sintering parameters (time, temperature, atmosphere, etc). The DSC/TGA thermo-grams were recorded using an automatic micro thermal analyzer (Netzsch STA 449 Thermal analysis instrument) in air at a constant heating rate of 10°C per minute. The dried powder obtained was calcined in air at 800°C for 4 h to yield the nano-sized oxide particles. The sintering temperature was selected by taking into account the relatively low melting point of Bi_2O_3 i.e., 825°C. The crystal phase analysis of the calcined samples was carried out at room temperature with an X-ray Diffractometer Diffrac Bruker AXS, D8 Advanced Plus, at 30 mA and 35 kV, with monochromatic CuK_α radiation, of wavelength λ= 1.5450Å. A scanned range 15-80° 2θ, with a step width of 0.02° were used. To obtain defined peaks it was necessary to use 15 sec as a count time per step and small grids, i.e. 0.2 mm. As this was only a phase identification method, no internal standard was added to the samples and phase identification with the

ICDD-PDF database. The average crystallite sizes D of the synthesized powders were estimated using Debye Scherrer formula and lattice parameters were determined from Rietveld refinement as implemented in Crystal Sleuth software. Surface morphology of the samples were analyzed at room temperature under accelerating voltage of 20kV with a scanning electron microscope (SEM) Leica- Cambridge, Stereoscan 440.

Results and Discussion

Thermal Analysis

The combined DSC-TGA curves in Figs. 1 (a)-(c) represent the breakdown behavior of the individual metal hydroxides. It can be seen that the putrefaction of $Zr(OH)_4$ takes place in two stages (blue curves Figs. 1a-c). The endothermic peak at 130^{o}C represents the loss of adsorbed moisture in the co-precipitated powders. The peak at 210°C may be assigned to the volatilization of ammonia and n-propanol used during washing from the system. The subsequent endothermic peak at 260°C and the broad endothermic peak in the range 500°C-600°C correspond to the decomposition of $Bi(OH)_3$ and $Zr(OH)_4$ to their amorphous oxide states respectively. This is accompanied by considerable weight losses of 64.04%, 68.66% and 48.79% (black curves) which are complemented by the associated exothermic peaks at 100°C and 250°C for samples (a), (b) and (c). The onset of transformation into a stable monoclinic ZrO_2 phase is observed above 600°C up to a saturation temperature of 700°C. This is evident from the powder X-ray diffraction patterns for the samples and conforms to the work of Santos (2008) and coworkers; where the transformation to monoclinic ZrO_2 phase was observed above 600°C. The results indicate that the calcination temperature for the precipitated samples is 700°C and this corresponds to 49.38%, 60.57% and 73.61% losses in weight at 800°C. The results presented in figures 1(a)-(c) are in good agreement with the work led by Shankar (2007) in which the saturation (sintering) temperature was observed at 700°C.

Figure 1(d) shows exothermic peaks at 100°C and 200°C while endothermic peaks at 130°C and 220°C. Following these transformations is a considerable weight loss of 46.28% due to evaporation of moisture content. Transformation into tetragonal phase of ZrO_2 occurs above 600°C while the cubic Bi_2O_3 phase occurs above 700°C, but this is accompanied by a tetragonal Bi_2O_3 phase. This deduction is in accordance with the phase transformation of low

symmetry phase of Bi_2O_3 to higher symmetry phase above 727°C, which on cooling leads to possible formation of tetragonal and body centered cubic phases. The overall weight loss of 71.83% was observed at saturation temperature.

In fig. 1(e), the peaks at 100°C and 200°C are associated with exothermic transformations while those at 120°C and 220°C are associated with endothermic transformations (blue curve).

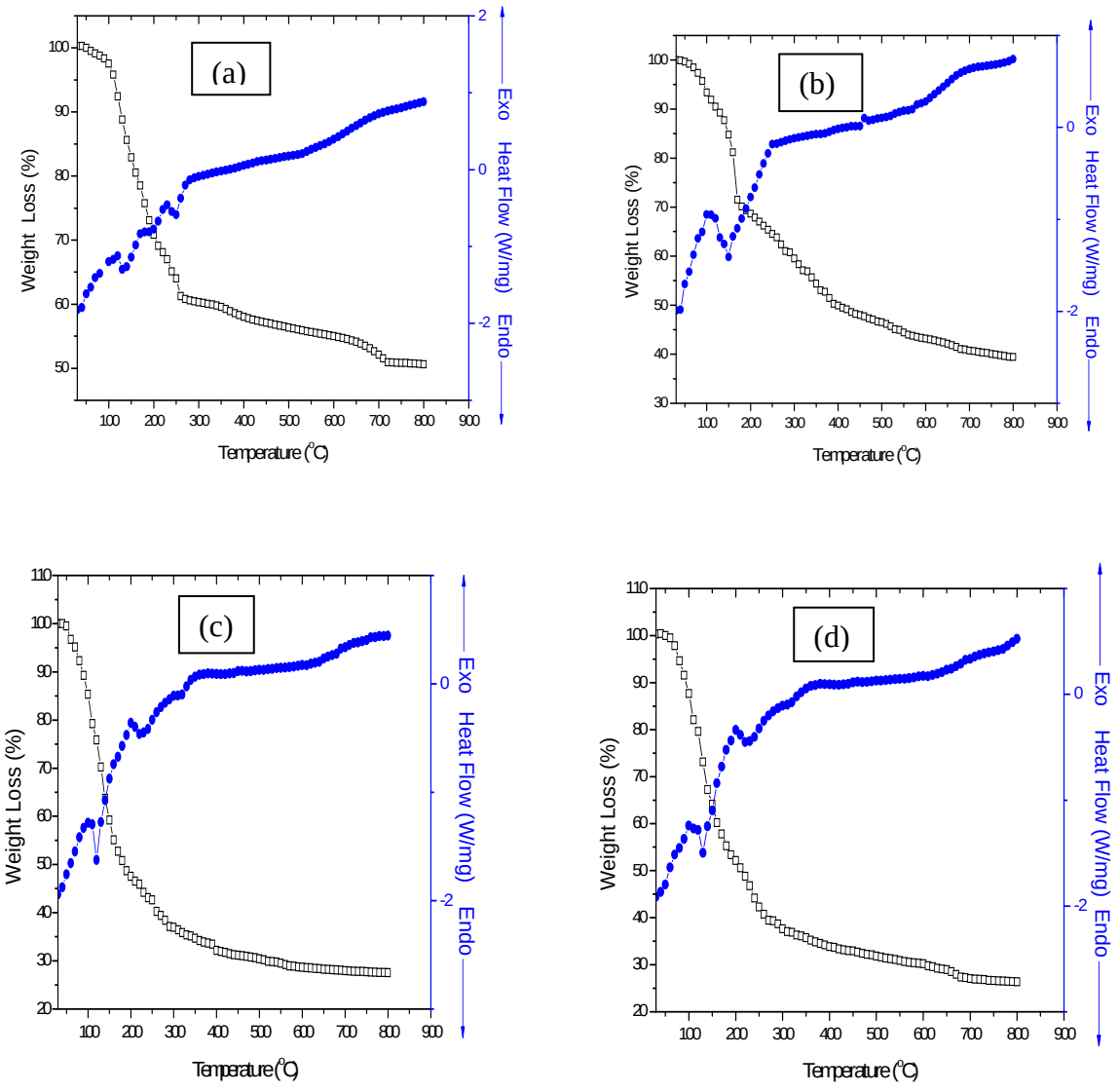

Figure 1. *Combined DSC-TGA for samples (a) 8BSZ (b) 12BSZ (c) 18BSZ, and (d) 40BSZ*

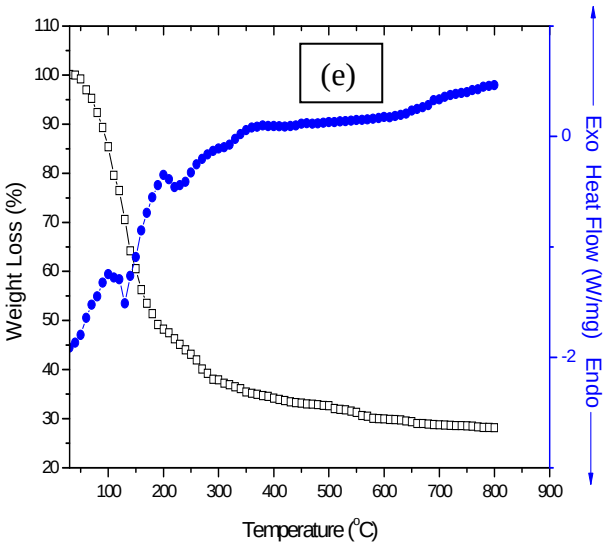

Figure 1. *Combined DSC-TGA for sample (e) 50BSZ*

The effect of these transformations corresponds to a weight loss of 45.89%. Phase transformations into monoclinic Bi_2O_3 and orthorhombic ZrO_2 phases occur at 330°C while the cubic Bi_2O_3 phase occurs above 700°C. A constant weight loss above the transformation temperature up to a saturation point is followed by an overall weight loss of 72.46%.

The thermo-gravimetric analysis (TGA) of the co-precipitated powders is in agreement with the DSC peaks showing distinct regimes of weight loss corresponding to the temperature regions mentioned in the DSC. The TGA of the co-precipitated powders shows a weight loss of more than 50% and most of it occurs below 500°C with a slight weight loss continuing up to 700°C. This large weight loss could be because of the dehydroxylation of hydroxides, conversion of metal chlorides into oxides as well as removal of excess NaCl from the system. In the temperature range 700°C -800°C, there is no significant weight loss reflecting that the saturation temperature for the co-precipitated powders is 700°C. This deduction fits well with the results of elemental analysis and XRD analysis.

XRD Analyses

X-ray diffraction analyses of the co-precipitated powder samples were carried out and the patterns are given in Figs. 2(a)-(e). The intense peaks in the XRD patterns of the co-precipitated powder samples lie in the angular (2θ) range of 15° and 80°. The patterns were

analysed and the peaks were identified using ICDD data file. It can be seen from the Figs. 2(a)-(c), that besides a very few minor peaks of bismuthoxychloride with low intensity, majority of the peaks belong to ZrO_2, indicating that the lattice structure of the mixed oxide matrix is primarily of ZrO_2 type. The XRD patterns of the co-precipitated powder samples in Fig. 2 (a) and (c) indicates that the intensity of the peaks (111) and (-111) is being modulated because of the presence of Bi_2O_3 in the ZrO_2 unit cell. This shows that the some of the dopant atoms occupy similar positions as the host atoms thereby leading to the dopant adopting the structure of the host matrix. The cause of lower intensity of the dopant phase may be attributed to its lower proportion (mole fraction) in the the co-precipitated powder samples as compared to host matrix. X-ray diffraction patterns of the as-synthesized co-precipitated powders (Fig.2 a-c) showed sharply defined peaks of BiOCl (JCPDS File card no. 6-0249) indicating its presence in a significant amount. In particular there are no peaks for any compounds, including chlorides and hydroxides of zirconium and sodium found in the co-precipitated powders. The diffraction pattern indicates that all such compounds may be present in the powders in an amorphous form.

The co-precipitated powders calcined at 800°C for 4 h showed crystallization peaks of BiOCl (JCPDS File card no. 6-0249) [14]. However, crystallization peaks of ZrO_2 of monoclinic symmetry were observed for co-precipitated powders calcined at 800^{o}C for 4 h, and the maximum peak in the diffraction pattern corresponded to the maximum peak position of crystalline ZrO_2 (ICDD File card no. 01-083-0937) [13]. The unit cell parameters for the monoclinic ZrO_2 were obtained from Rietveld least square refinement to be $a = 5.0792$ Å, $b = 5.2290$ Å and $c = 5.3385$ Å for co-precipitated powder sample (a), $a = 5.1734$ Å, $b = 5.2041$ Å and $c = 5.3420$ Å for co-precipitated powder sample (b) and $a = 5.1608$ Å, $b = 5.2288$ Å and $c = 5.3442$ Å for co-precipitated powder sample (c). The variation in the unit cell dimension is due to unit cell expansion as a result of incorporation of dopant with uncertainty in all cases less than 1%. The unit cell of BiOCl is tetragonal and the XRD peak positions varied slightly for the co-precipitated powder samples corresponding to variations in cell dimensions within the limits $a = 3.81 - 3.83$ Å, $c = 7.52 - 7.54$ Å and $c/a = 1.96 - 1.97$. The crystallite sizes of the co-precipitated powders were calculated from the peak broadening of X-ray diffraction patterns using Scherrer equation. The crystallite sizes were 29nm, 26nm and 21nm respectively for the co-precipitated powders calcined at 800^{o}C.

The XRD patterns for the as-synthesized co-precipitated powder samples containing

higher concentration of dopant shown in Fig. 2 (d) and (e) are quite different from those shown in Fig 2(a)- (c). In the co-precipitated powders, there is ample amount of chloride; so amorphous Bi_2O_3 may have reacted with chloride to form the BiOCl phase as per the following equation:

$$Bi_2O_3 + BiCl_3 \rightarrow 3BiOCl \quad (1)$$

The presence of BiOCl peaks in XRD pattern (Fig. 2d) suggests that BiOCl is a very stable chloride in comparison with sodium chloride, and this may have delayed the formation of ZrO_2 and Bi_2O_3 phases. The decrease in intensity of BiOCl peaks in the diffraction patterns indicates the gradual disappearance of that phase. This may have occurred as per the following reaction:

$$4BiOCl + O_2 \rightarrow Bi_2O_3 + 2Cl_2 \quad (2)$$

Though the system takes oxygen from the atmosphere, there is also a loss of 2 mol of chlorine for every mole of oxygen coming into the system. This is well supported by a small and continued weight loss at higher temperatures in the TGA curve. The unit cell parameters of tetragonal ZrO_2 were calculated to be $a = 3.6177\,\text{Å}$, $c = 5.6500\,\text{Å}$ and $c/a = 1.5618$ while that for tetragonal BiOCl ($a = 3.84 - 3.85\,\text{Å}$, $c = 7.53 - 7.54\,\text{Å}$ and $c/a = 1.95 - 1.96$) [14]. The crystallite sizes were 8nm, 15nm and 33nm respectively for the different phases present in the co-precipitated powders calcined at 800^{o}C.

Finally, the XRD pattern for the co-precipitated powder sample shown in Fig. 2(e) is very complicated. The presence of chlorine in the system as BiOCl might have reacted with the amorphous Bi_2O_3 to form this phase. However, crystallization peaks of Bi_2O_3 of monoclinic and tetragonal symmetries were observed for co-precipitated powders calcined at 800^{o}C for 4 h, and the maximum peak in the diffraction pattern corresponded to the maximum peak position of crystalline tetragonal Bi_2O_3 (ICDD File card no. 01-076-2477) [13]. The presence of BiOCl peaks in XRD pattern (Fig. 2e) suggests that bismuthoxychloride is a very stable chloride in comparison with sodium chlorides, and this may have delayed the formation of ZrO_2 and Bi_2O_3 phases. The decrease in intensity of chlorides of bismuth peaks in the diffraction patterns indicates the gradual disappearance of that phase and this is in accordance with the above equation (2) and the fact that the percentage weight of chlorine (11.41%) is small compared with that in the co-precipitated sample (d). This is well supported by the

small percentage of chlorine in comparison with other samples in the EDS analysis (Table 1).The unit cell parameters of orthorhombic ZrO_2 were calculated to be $a = 3.6177$ Å, $b = 6.5216$ Å and $c = 7.5121$Å while that for tetragonal BiOCl is $a = 3.85$ Å, $c = 7.52$ Å and $c/a = 1.95$. For the tetragonal Bi_2O_3 phase $a = 3.6640$ Å and $c = 20.7269$Å while that for the monoclinic Bi_2O_3 phase is $a = 5.9596$ Å, $b = 8.1644$ Å and $c = 7.5121$Å. The crystallite sizes were 9nm, 15nm, 12nm and 14nm respectively for the different phases present in the co-precipitated powders calcined at 800^{o}C.

Scanning Electron Microscopy and EDS Analyses

The microstructural investigations of the co precipitated powders in the system $(ZrO_2)_{1-x}$:$(Bi_2O_3)_x$ were carried out and the micrographs for the stabilized zirconia are presented in Fig. 3 (a)-(e) which shows that the grains are interspersed with the ZrO_2 particles.

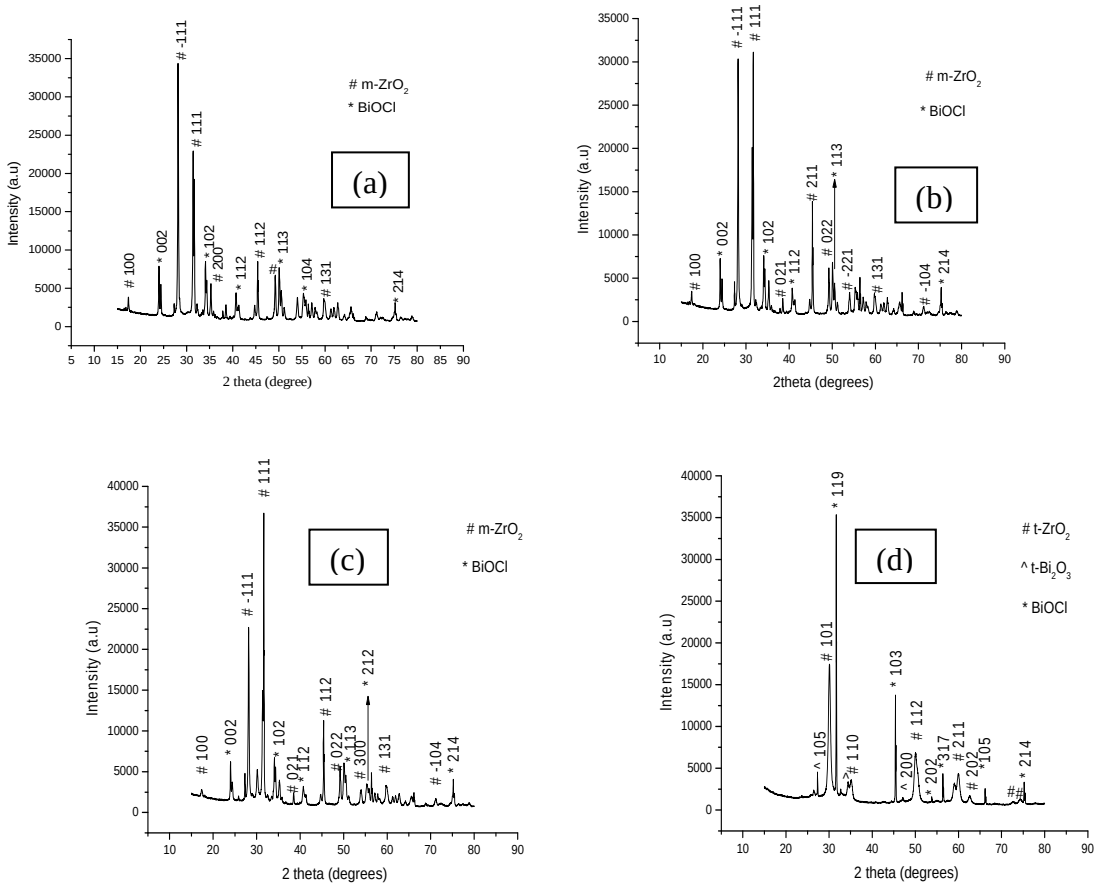

Figure 2. *X-Ray Diffraction patterns for samples (a) 8BSZ, (b) 12BSZ, (c) 18BSZ, and (d) 40BSZ*

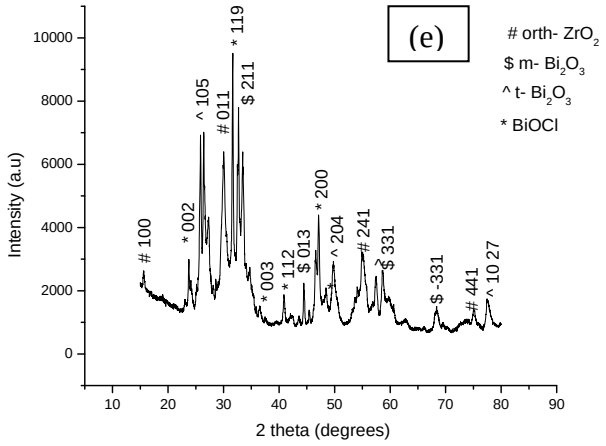

Figure 2. *X-Ray Diffraction patterns for sample (e) 50BSZ*

The development of interfaces can also be predicted qualitatively from the micrograph (Fig. 3). However, the existence of ZrO_2 as a separate phase was noticed as a common feature.

The mixed oxide grains can also be contrasted as the Bi_2O_3 appearing as dark grain is overlaid by much clustered ZrO_2 in lighter contrast. The contrast observed in the mixed oxide phase arises from two principal sources: first, the lightness of the zirconia phase compared with darker bismuth oxide background is mostly due to the difference in secondary electron yield of the two phases. Zirconia being less conducting has much the higher yield. The second cause of contrast is topographical, arising from the angular variations that the zirconia phase makes with the incident beam. In Figs. 3(a) and 3(b), the particles are nearly spherical in shape and the distribution of the particles is such that they are closely packed together. The average particle size is determined from SEM with imaging software (Image-J) to be 101±4μm and 94±4μm respectively. The microstructure in figure 3(c) shows clear boundary between the agglomerated grains of the mixed oxide phase with ZrO_2 particles interspersed on the surface of the grains and along the grain boundaries. The average particle size is determined from SEM with imaging software (Image-J) to be 63±3μm. Even though the microstructure for co-precipitated samples in Figs. 3(d) and 3(e), appear distinct, the development of interfaces can also be predicted qualitatively from the micrographs. However, the existence of ZrO_2 as a separate phase was noticed as a common feature but the mixed oxide phase appears much more agglomerated with plate like formation. Qualitatively, the ZrO_2 phase is interspersed on the platy grains of the mixed oxide and along the interfaces.

The average particle size is determined from SEM with imaging software (Image-J) to be 75±4μm and 67±2μm respectively. In conclusion, the morphology of the synthesized solid electrolytes revealed that the particles are nearly spherical in shape and with little agglomeration for samples shown Figs 3 (a)-(c) while for samples in Figs. 3(d) and (e) there is much more agglomeration leading to plate-like formation. The average particle size decreases with increase in volumetric concentration of dopant (Bi_2O_3) with a broad particle size distribution.

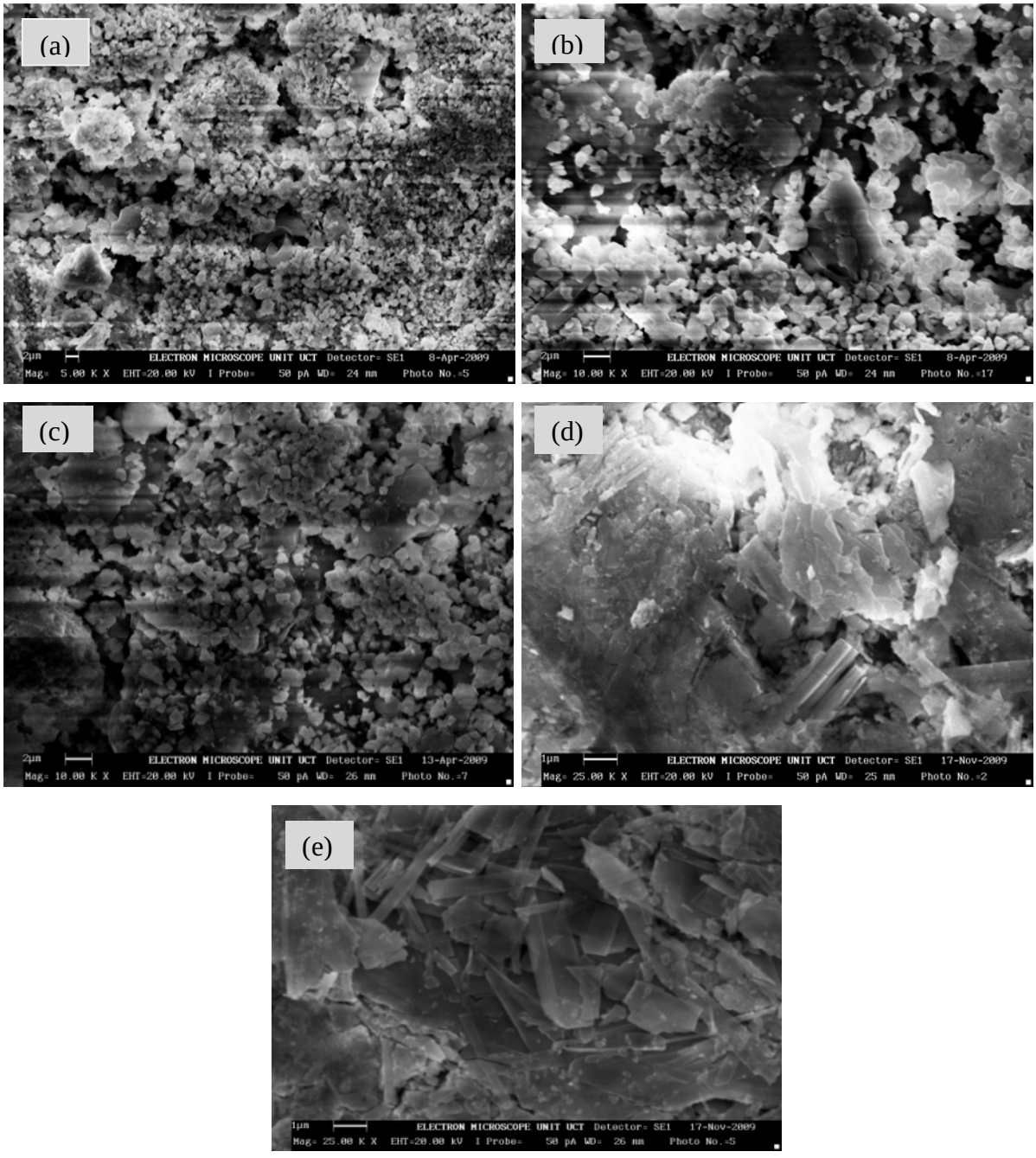

Figure 3. *Typical Scanning Electron Micrograph (SEM) for Samples (a) 8BSZ, (b) 12BSZ, (c)*

18BSZ, (d) 40BSZ, and (e) 50 BSZ

The X-ray microanalysis confirmed the presence of zirconium, bismuth, oxygen, sodium and chlorine as the components of the co-precipitated powder samples. Zirconium and bismuth were detected with higher relative concentrations compared to the other components. The quantitative analytic results for the co-precipitated powder samples are presented in Table 1.

Table 1. Sodium and Chlorine contents in the Stabilized Zirconia Solid solutions

Sample	Sodium (%)	Chlorine(%)
a	1.94	18.34
b	6.10	18.01
c	1.66	18.88
d	-	30.69
e	-	11.41

The chlorine content ranges from 11.41% to 30.69%. The chlorine content in the co-precipitated powders can be associated to the presence of NaCl, $BiCl_3$, BiOCl and $ZrCl_4$. Furthermore, the microanalysis of the co-precipitated powder sample (d) indicates 30.69% of Cl content, which may only be due to any chloride form of zirconium and bismuth as the chlorides of ammonium and sodium are not stable at high temperatures.

This suggests that the co-precipitated powder has a significant amount of entrapped unreacted chlorides of zirconium and bismuth during precipitation process. The same reason could also be extended to the entrapment of NaCl in the precipitates for co-precipitated powder samples (a)-(c) as chlorine content is significantly high. In contrast, the microanalysis of the co-precipitated powder samples (d) and (e) did not indicate the presence of sodium; this elimination may be due to excessive washing with doubly distilled water as it is easier to get rid of sodium compared to chlorine. The reduction in chlorine content in the co-precipitated powder sample (e) might be owed to the fact that greater percentage of bismuth chloride is converted to its oxide as compared to that of zirconium. The same logic could also be extended to the conversion of chloride of zirconium in preference to that of bismuth in the other co-precipitated powder samples.

Conclusions

The co-precipitated stabilized zirconia powders were synthesized via a wet chemical route with optimum sintering temperature of 700^{o}C. The phase transformation form amorphous state to crystalline state for the stabilized zirconia occurred above 600°C for the monoclinic zirconia and above 700°C for the bismuthoxide. The X-Ray Diffraction analyses showed that BiOCl phase is a stable crystalline phase because the chloride of bismuth is more stable compared to the chloride of sodium. The average crystallite sizes for the phases contained in the stabilized zirconia powders spans the range of 8-33nm. The microstructure of the stabilized zirconia powders as obtained from SEM analysis revealed that the particles are nearly spherical in shape and had broad particle size distribution with little agglomeration and porosity. The particle size increases with increase volumetric concentration of dopant with values ranging from 63-101µm. Finally, EDS analysis confirmed the presence of Zirconium, bismuth, chlorine, sodium and oxygen as the components of the co precipitated powders with zirconium having higher concentration in all the samples except the sample (e) with 11.41% of chlorine and no traces of sodium.

References

1. Ahmed T. O., Akusu P. O., Jonah S. A., Rabiu N., Abdelmalik A. A., Zubairu S. M. J., *Synthesis and Structural Evaluation of Nanocrystalline Bismuth Oxide Stabilized Zirconia for Intermediate-Temperature Solid Oxide Fuel Cells*, Fifth International Conference of the African Materials Research Society, Sheraton Hotels, Abuja, Nigeria, 2009, p.140.
2. Georges S., Goutenoire F., Bohnke O. Steil M. C., Skinner S. J., *The LAMOX Family of Oxide-Ion Conductors: Over-view and Recent Results*, Journal of New Materials for Electro-Chemical Systems, 2004, 7, p. 51-57.
3. Srikant E., Bichile G. K., *Synthesis and structural Characterization of* $(Bi_2O_3)_{1-x}(Y_2O_3)_x$ *and* $(Bi_2O_3)_{1-x}$ $(Gd_2O_3)_x$ *solid solutions*, Bull. Mater. Sci., 2004, 27(1), p.19-22.
4. Dudek M., Molenda J., *Ceria-yttria-Based Solid Electrolytes for Intermediate Temperature Solid Oxide Fuel Cells*, Materials Science-Poland, 2006, 24(1), p.45-52.

5. Tok A. I. Y., Luo L. H., Boey F. Y. C., *Consolidation and Properties of* $Gd_{0.1}Ce_{0.9}O_{1.95}$ *Nanoparticles for Solid Oxide Fuel Cell Electrolytes*, J. Mater., 2006, 21(1), p. 119-124.
6. Zhong G. H., Wang J. L., Zeng Z., *Ionic Transport Properties in Doped* $\delta - Bi_2O_3$, Journal of Physics: Conference Series 29; 3rd Conference of the Asian Consortium for Computational Materials Science, 2006, p. 106-109.
7. Haering C., Roosen A., Schichl H., *Degradation of the Electrical Conductivity in Stabilized Zirconia Systems: Part II: Scadia Stabilized Zirconia*, Solid State Ionics, 2005, 176, p. 261-268.
8. Lei Z., Zhu Q., *Low Temperature Processing of Dense Nanocrystalline Scandia doped Zirconia (ScSZ) Ceramics*, Solid State Ionics, 2005, 176(37-38), p. 2791-2797.
9. Shankar S. R., Jayakanth R., Maiti S., Kumar A., Manna I., *Synthesis and Characterization of Nanocrystalline Dysprosia Stabilized Zirconia for Intermediate-Temperature Solid Oxide Fuel Cells*, Material Science Eng. B., 2007, p.1-14.
10. Zhu W. Z., *Effect of Cubic Phase on the Kinetics of the Isothermal Tetragonal to Monoclinic Transformation in* $ZrO_2(3mol\%Y_2O_3)$ *Ceramics*, Ceramics International, 1998, 24, p. 35-43.
11. Santos V., Zeni M., Bergmann C. P., Hohemberger J. M., *Correlation between Thermal Treatment and Tetragonal/Monoclinic Nanostructured Zirconia Powder Obtained By Sol-Gel Process*, Rev. Adv. Mater. Sci., 2008, 17, p. 62-70.
12. Radha A. V., Oscar B. M., Sergey V. U., Alexandra N., Pedro T., *Surface Enthalpy, Enthalpy of Water Adsorption and Phase Stability in Nanocrystalline Monoclinic Zirconia*, J. Am. Ceram. Soc., 2009, 92(1), p. 133-140.
13. Ahmed T. O., *Synthesis and Structural Evaluation of* $(ZrO_2)_{1-x}(Bi_2O_3)_x$ *Solid Electrolytes.* Unpublished PhD Dissertation, Department of Physics, Ahmadu Bello University, Zaria, Nigeria, 2010, p. 1-184
14. Swansonr H. E., Fuyat K., Ugrinic G. M., *Natl. Bur. Stand. (U.S.) Circ. No. 539, (JCPDS File Card. No. 6-0249)*, 1955, 4, p. 54.